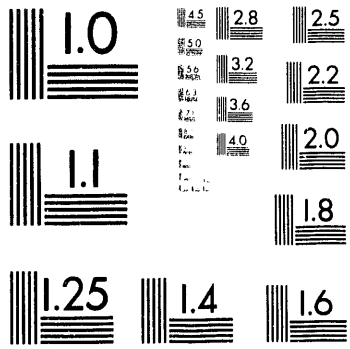
1.0
1.1
1.25
1.4
1.6
1.8
2.0
2.2
2.5
2.8
3.2
3.6
4.0
4.5
5.0
5.6

1 of 1

BEAM POSITION FEEDBACK SYSTEM FOR THE ADVANCED PHOTON SOURCE*

Y. Chung
Argonne National Laboratory, Argonne, IL 60439

ABSTRACT

The Advanced Photon Source (APS) will implement both global and local beam position feedback systems to stabilize the particle and X-ray beams for the storage ring. The systems consist of 20 VME crates distributed around the ring, each running multiple digital signal processors (DSP) running at 4kHz sampling rate with a proportional, integral, and derivative (PID) control algorithm. The particle and X-ray beam position data is shared by the distributed processors through networked reflective memory. A theory of closed orbit correction using the technique of singular value decomposition (SVD) of the response matrix and simulation of its application to the APS storage ring will be discussed. This technique combines the global and local feedback systems and resolves the conflict among multiple local feedback systems due to local bump closure error. Maximum correction efficiency is achieved by feeding back the global orbit data to the local feedback systems. The effect of the eddy current induced in the relatively thick (1/2") vacuum chamber by the AC corrector magnet field for local feedback systems is compensated by digital filters. Results of experiments conducted on the X-ray ring of the National Synchrotron Light Source and the SPEAR at Stanford Synchrotron Radiation Laboratory will also be presented.

INTRODUCTION

The third generation synchrotron light sources, of which the Advanced Photon Source (APS) is one, are characterized by low emittance of the charged particle beams and high brightness of the photon beams radiated from insertion devices. Transverse stability of the particle beams is a crucial element in achieving these goals and the APS will implement extensive beam position feedback systems, which include 320 corrector magnets, 360 positron beam position monitors (BPMs)

Table 1. Specification of the beam position feedback systems.

	Global DC	Global AC	Local
Orbit measurement device	All of the RF BPMs	RF BPMs (1/sector)	RF BPMs X-ray BPMs
Correctors	All correctors (320)	Subset of correctors	Local bump
Specified orbit measurement resolution	25 μm	25 μm	1 μm
Achievable resolution	5 μm	5 μm	1 μm
Required range of correction	± 20 mm	± 500 μm	± 100 μm

*Work supported by the U.S. Department of Energy, Office of Basic Energy Sciences, under Contract No. W-31-109-ENG-38.

distributed around the storage ring of 1104 m circumference, miniature BPMs for insertion device beamlines, and photon beam position monitors in the front end of X-ray beamlines. The beam position feedback systems are largely divided into the global and local feedback systems according to the extent of correction, and the DC and AC feedback systems according to the bandwidth of correction.[1-4] Table 1 shows the specification of the beam position feedback systems to be employed in the APS storage ring.

The APS beam position feedback system is characterized by: (1) digital implementation with proportional, integral, and derivative (PID) control, (2) orbit correction algorithm based on singular value decomposition (SVD) of the response matrix, and (3) combination of the global and local feedback systems into a single, unified system for maximum correction efficiency and orbit stability. These key aspects will be discussed in three parts of this paper. In the first part, we will overview Z-transform and the theory of digital signal processing and discuss compensation for the vacuum chamber eddy current effect. In the second part, the global orbit correction experiments conducted at NSLS and SSRL and analysis of the APS storage ring based on the SVD algorithm will be discussed. The hardware and software configuration for the APS beam position feedback system will be discussed in the last part.

DIGITAL SIGNAL PROCESSING

In order to avoid the problems characteristic of analog circuits, e.g., drift, offset, and sensitivity to temperature change, we will use digital signal processing (DSP) for beam position feedback. This also provides added flexibility through user programmability. The BPM processors distributed around the ring transfer the beam position data in digital format to the feedback system. The digital signal processors then calculate the corrector strengths and control the corrector power supplies. The updated beam positions are then read by the BPMs again, and the feedback cycle continues at a given sampling frequency. In this section, we will discuss theory of digital closed loop feedback and its application to compensation for the effect of eddy current in the vacuum chamber.[5-7]

A. Digital Filters

Just as the Fourier transform and the Laplace transform are important in continuous-time signals and systems, Z-transform facilitates the analysis of discrete-time signals and systems.[6] Given a sequence of discrete-time signals $\{x_n\}$, its Z-transform is defined by

$$X(z) = \sum_{n=-\infty}^{\infty} x_n z^{-n} \tag{1}$$

where z is a complex variable and plays a role similar to that of the variable s in the Laplace transform. $\{x_n\}$ is called the inverse transform of X(z).

For a discreet input sequence $\{x_n\}$ sampled at every T, a digital filter produces an output sequence $\{y_n\}$ given by the difference equation

$$y_n = \sum_{k=0}^{M} a_k x_{n-k} - \sum_{k=1}^{L} b_k y_{n-k}\ , \tag{2}$$

where $\{a_k\}$ and $\{b_k\}$ are the filter coefficients. F_s (= 1/T) is the sampling frequency. The filter takes M previous inputs plus the current one and L previous outputs, and

therefore, the filter is physically realizable or causal. Performing a Z-transform on Eq. (2), we obtain

$$Y(z) = H(z)X(z), \tag{3}$$

where X(z) and Y(z) are the Z-transforms of $\{x_n\}$ and $\{y_n\}$ and H(z) is the filter function given by

$$H(z) = \frac{\sum_{k=0}^{M} a_k z^{-k}}{1 + \sum_{k=1}^{L} b_k z^{-k}}. \tag{4}$$

With $z = e^{-i\lambda}$ and $\lambda = \pi f/F_s$, the Z-transform is the digital analog of the Fourier transform.

The inverse of the filter H(z) in Eq. (4) can be written as

$$\frac{1}{H(z)} = \frac{1}{a_0} \frac{\sum_{k=0}^{L} b_k z^{-k}}{1 + \sum_{k=1}^{M} \frac{a_k}{a_0} z^{-k}}. \qquad (b_0 = 1) \tag{5}$$

The inverse filter given by Eq. (5) can be used to compensate for analog devices if the corresponding filter coefficients $\{a_k\}$ and $\{b_k\}$ can be obtained by fitting the frequency response to Eq. (4) with $z = e^{-i\lambda}$. We will use this approach to compensate for the effect of eddy current in the vacuum chamber.

B. Closed Loop Feedback with DSP

In designing the digital signal processing scheme for closed loop feedback, the following factors must be considered:

- Rise-time
- Overshoot
- Settling time
- Control effort
- Noise throughput

The major parameters that determine the performance of the closed loop feedback are controller gains, open loop bandwidth, and sampling frequency. In the following, we will discuss these parameters and closed loop feedback using DSP.

In Fig. 1 is shown a simple closed loop feedback system with proportional control of open loop constant gain G. The bandlimiting filter (BLF), inserted in the loop for stability reasons, is a low-pass filter with bandwidth f_b and has the filter function

$$B(z) = \frac{1 + z^{-1}}{1 + c + (1 - c)\, z^{-1}}. \qquad c = \cot\left(\frac{\pi f_b}{F_s}\right) \tag{6}$$

The response of the system in the form of a difference equation is given by

$$(1 + c)\, y_{n+1} + (1 - c + G)\, y_n + G\, y_{n-1} = G\,(s_n + s_{n-1}). \tag{7}$$

Assuming $F_s >> f_b$, Eq. (7) can be converted to a second-order differential equation and Fourier analyzed for stability according to the location of two poles in the complex frequency plane. In general, a closed loop feedback system with k open loop poles can be represented as a filter with k+1 poles.

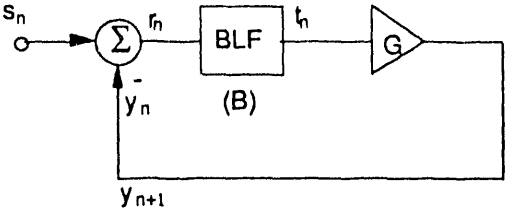

Fig. 1: Closed loop feedback with digital signal processing. BLF is the bandlimiting filter with bandwidth of f_b.

The system is stable if $G < 1 + c$ and, assuming $G >> 1$, the bandwidth of the closed loop system is approximately equal to $G f_b$. It can be shown that the condition for critically damped response to a step impulse is

$$\frac{F_s}{G f_b} \approx 20, \tag{8}$$

and therefore, the bandwidth of the optimally controlled feedback system is roughly equal to $F_s/20$.

C. Compensation for the Effect of Vacuum Chamber Eddy Current

The AC corrector magnets, which will correct beam motion of up to 100 μrad at 25 Hz, induce eddy current in the relatively thick (1/2") aluminum vacuum chamber of the storage ring for the local beam position feedback systems. This results in significant attenuation and phase shift of the magnet field even at frequencies as low as 5 Hz. Compensation for this effect can be done by inserting a digital filter in front of the power supply control interface, which closely approximates the inverse of the vacuum chamber and compensates for the eddy current effect. The global orbit feedback system uses a thin stainless steel chamber and is not significantly affected by the eddy current effect.

For measurements of the eddy current effect and its compensation, a prototype of the storage ring sextupole magnet was used, which has geometry similar to that of the six-pole horizontal/vertical corrector magnet as shown in Fig. 2. The effect of the eddy current in the 0.025"-thick magnet laminations was measured and found to be negligibly small in a previous work.[8] In Figs. 3(a) and 3(b) are shown the attenuation and phase shift of the field relative to the magnet current as functions of frequency at the center of the vacuum chamber ($x = y = 0$). The vertical field shows stronger attenuation and phase shift with frequency than the horizontal field, though the horizontal field appears to catch up in the high frequency region.

Besides field attenuation and phase shift, the vacuum chamber eddy current significantly changes magnet resistance and inductance. For the horizontal field, they changed from 100 mΩ and 11.8 mH at DC to 920 mΩ and 8.2 mH at 200 Hz. For the vertical field, the changes were from 80 mΩ and 8.7 mH at DC to 460 mΩ and 4.9 mH at 200 Hz. While this has the effect of reducing the magnet time constant, it also increases power consumption.

Spatially resolved measurement of the vertical magnet field in the vacuum chamber shows significant multipole components. Below 20 Hz, the quadrupole component dominates ($|b_1| \approx 0.12$ cm^{-1} @ 20 Hz), while above 50 Hz the sextupole component becomes stronger ($|b_2| \approx 0.16$ cm^{-2} @ 100 Hz). These multiple components will cause local bump closure error in the local feedback systems and result in interference among them. This effect will be resolved by global orbit feedback.

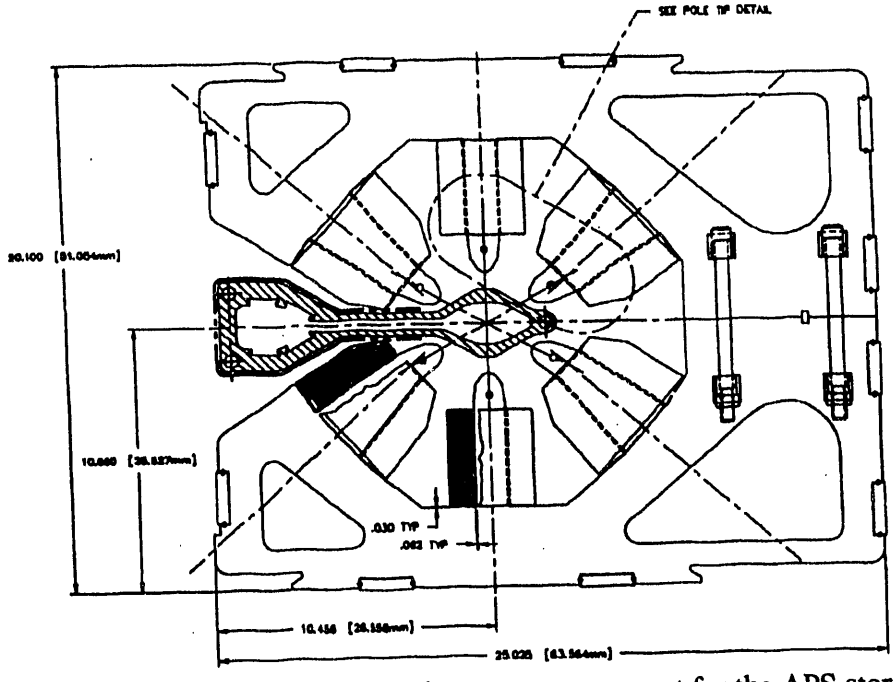

Fig. 2: The horizontal/vertical combination corrector magnet for the APS storage ring.

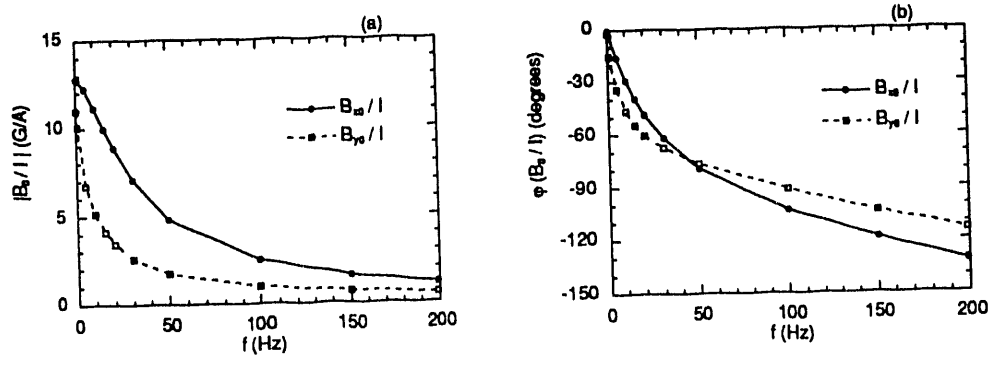

Fig. 3: (a)Attenuation of the field efficiency $|B_{x,y0}/I|$ and (b) phase shift φ between the field and the current as functions of frequency at the center of the vacuum chamber (x = y = 0).

D. Closed Loop Feedback with PID Control

Figure 4 shows the schematic diagram for closed loop feedback with PID control for the magnet field in the vacuum chamber. A bandlimiting filter (BLF) of 30 Hz was used for the measurements. The analog reconstruction filter (ARF) is an analog low pass filter of 200-Hz bandwidth inserted in front of the power supply control input in order to eliminate high frequency components in the discreet output from DSP. It was also intended to simulate the X-ray BPM with finite bandwidth. ARF was used only for closed loop measurements.

For the open loop measurements of the frequency response, the control signal is at either the input of the CF (u_n) or the PS (x_n) in Fig. 4. For the closed loop measurements, the control signal is at the input of the DSP (s_n). The digital compensation filter (CF) was obtained by inverting the digital filter representation of the vacuum chamber. Using the measurement results shown in Fig. 3(a), the best fit with four poles and four zeroes gives

$$q_n = 57.8\,(u_n - 3.1575996823\,u_{n-1} + 3.5206625349\,u_{n-2} - 1.56793656962\,u_{n-3} + 0.2048748912\,u_{n-4}) + 1.60395604698\,q_{n-1} - 0.276518570415\,q_{n-2} - 0.30381547655\,q_{n-3} - 0.023772023183\,q_{n-4}. \quad (9)$$

Since no future samples from either the input or output are needed to calculate the current output, the filter is physically realizable or causal.

The results of measurements on B_{y0}/B_c (B_c: control signal) with and without CF are shown in Fig. 5. Figure 6 shows time domain measurements of the magnet field B inside the vacuum chamber in response to the input square pulses of 15 Hz with the CF turned off and on.

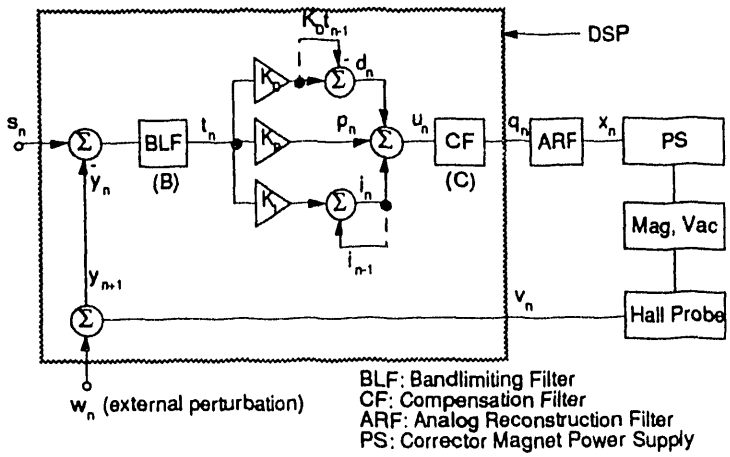

Fig. 4: Schematic diagram for the closed loop feedback with PID control.

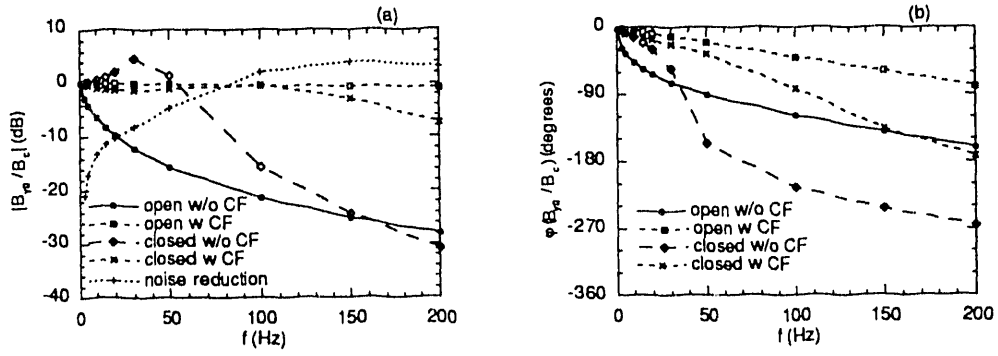

Fig. 5: Results of measurements on the closed loop feedback for the corrector magnet field: (a) amplitude attenuation and (b) phase shift. The parameters used were: $F_s = 4$ kHz, $f_b = 30$ Hz, $K_P = 3$, $K_I = 0.05$, and $K_D = 0.5$.

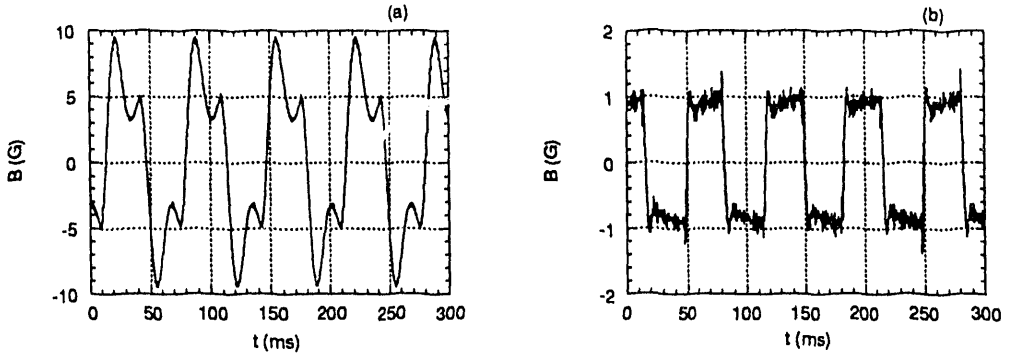

Fig. 6: Feedback system response in the time domain (a) without and (b) with eddy current compensation. The parameters used were: F_s = 4 kHz, f_b = 30 Hz, K_P = 3, K_I = 0.05, and K_D = 0.5. The control signal is a 15-Hz square wave of ±5G for (a) and ±1G for (b).

ORBIT CORRECTION ALGORITHM

The orbit correction algorithm for the beam position feedback systems is based on the analysis of the response matrix using the technique of singular value decomposition (SVD) of matrices. The response matrix relates the beam motion at selected BPMs and changes in corrector strengths. SVD transforms the response matrix into a diagonal matrix, with the diagonal elements representing the correction efficiency of non-interacting orbit correction channels. The AC orbit correction is then equivalent to a combination of the DC correction algorithm and multiple non-interacting feedback systems.

The mathematical formulation of the SVD of matrices is broadly available in the literature[9-12] and its successful application to closed orbit correction at Aladdin, SRC, was reported in Ref. 13. In this section, we will overview the SVD formalism and its application to closed orbit correction.[14]

A. SVD Formalism

Let us consider M BPMs and N correctors used for closed orbit correction in the storage ring. The i-th BPM has beta and phase functions (β_i, ψ_i), and similarly, the j-th corrector has (β_{cj}, ψ_{cj}). The response matrix R_{ij} corresponding to the beam motion at the i-th BPM per unit angle of kick by the j-th corrector is then given by[15]

$$R_{ij} = \frac{\sqrt{\beta_i \beta_{cj}}}{2 \sin \pi\nu} \cos\left(|\psi_i - \psi_{cj}| - \pi\nu\right). \tag{10}$$

ν is the betatron tune of the machine. The response matrix R_{ij} can be measured by reading beam position changes while varying the corrector strengths one by one.

We write the response matrix $\mathbf{R}$ as a product of three matrices $\mathbf{U}$, $\mathbf{W}$, and $\mathbf{V}$ as[12]

$$\mathbf{R} = \mathbf{U} \cdot \mathbf{W} \cdot \mathbf{V}^T, \tag{11}$$

where $\mathbf{U}$ is an M × M unitary matrix ($\mathbf{U}^T \cdot \mathbf{U} = \mathbf{U} \cdot \mathbf{U}^T = \mathbf{1}$), $\mathbf{W}$ is an M × N diagonal matrix with positive or zero elements, and $\mathbf{V}$ is an N × N unitary matrix ($\mathbf{V}^T \cdot \mathbf{V} = \mathbf{V} \cdot \mathbf{V}^T = \mathbf{1}$). This decomposition is unique only to a certain extent, and there are other ways of decomposing the matrix $\mathbf{R}$.[16,17]

Let us denote by Δx the global orbit change due to the corrector strength change $\Delta\boldsymbol{\theta}$ and define

$$\Delta \mathbf{x}^t = \mathbf{U}^T \cdot \Delta \mathbf{x} \quad \text{and} \quad \Delta \boldsymbol{\theta}^t = \mathbf{V}^T \cdot \Delta \boldsymbol{\theta}. \tag{12}$$

Then, from Eqs. (11) and (12) we have

$$\Delta \mathbf{x}^t = \mathbf{W} \cdot \Delta \boldsymbol{\theta}^t. \tag{13}$$

Equation (12) is the rule of transformation for the BPMs and correctors. $\Delta \mathbf{x}^t$ and $\Delta \boldsymbol{\theta}^t$ are the vectors in the transformed BPM (t-BPM) space and transformed corrector (t-corrector) space, respectively. The columns of the matrices **U** and **V** are the orthogonal basis vectors $\{\mathbf{u}_i\}$ and $\{\mathbf{v}_j\}$. The elements of the matrix **W** are given by

$$W_{ij} = w_{\min(i,j)}\, \delta_{ij}\,. \tag{14}$$

We call these diagonal elements w_n (≥ 0, $1 \leq n \leq \min(M, N)$) eigenvalues, which represent the coupling efficiency between the t-BPMs and t-correctors. The matrix **R** is singular if any of the eigenvalues are equal to zero. The basis vectors are related through the relation

$$\mathbf{R} \cdot \mathbf{v}_n = w_n\, \mathbf{u}_n\,. \qquad 1 \leq n \leq \min\,(M, N) \tag{15}$$

B. Matrix Inversion and Orbit Correction

Let $\Delta \mathbf{x}$ be the orbit error given by the difference between the reference orbit $\mathbf{x}_r$ and the current orbit $\mathbf{x}_m$. That is,

$$\Delta \mathbf{x} = \mathbf{x}_r - \mathbf{x}_m\,. \tag{16}$$

In order to bring the orbit to the reference orbit, we need to calculate $\Delta\boldsymbol{\theta}$ such that

$$\mathbf{R} \cdot \Delta \boldsymbol{\theta} = \Delta \mathbf{x}. \tag{17}$$

In case such solutions do not exist, we want the solution that minimizes the difference $|\mathbf{R} \cdot \Delta\boldsymbol{\theta} - \Delta \mathbf{x}|$. SVD provides this solution as

$$\Delta \boldsymbol{\theta} = \mathbf{R}_{inv} \cdot \Delta \mathbf{x}, \tag{18}$$

where

$$\mathbf{R}_{inv} = \mathbf{V} \cdot \mathbf{W}_{inv} \cdot \mathbf{U}^T. \tag{19}$$

$\mathbf{W}_{inv}$ is a diagonal matrix of dimension $N \times M$ and the elements are given by

$$W_{inv,ij} = q_{\min(i,j)}\, \delta_{ij}\,, \tag{20}$$

where

$$q_n = \begin{cases} 0, & w_n \leq \varepsilon w_{max} \\ \dfrac{1}{w_n} & \text{otherwise.} \end{cases} \qquad (1 \leq n \leq \min\,(M, N)) \tag{21}$$

ε is the singularity rejection parameter in the range [0,1]. This parameter is determined primarily by the orbit correction needs and the corrector strength limits. Zero q_n's correspond to decoupled channels which do not contribute to orbit correction.

When $\varepsilon = 0$, all the non-zero eigenvalues are retained and the most accurate correction will result. However, this will require very robust power supplies for the correctors. On the other hand, if $\varepsilon = 1$, $\mathbf{R}_{inv}$ is a null matrix then there will be no orbit

correction. Usually, ε is set to the smallest value such that none of the power supplies saturates.

For a given matrix $\mathbf{R}$, we define $\varepsilon_m(\mathbf{R})$ as

$$\varepsilon_m(\mathbf{R}) = \max \{\varepsilon \mid w_n > \varepsilon\, w_{max} \text{ for all } w_n \neq 0\}. \tag{22}$$

That is, ε_m is the largest possible value for ε in order to retain all non-zero eigenvalues. The inverse matrix $\mathbf{R}_{inv}$ satisfies

$$\mathbf{R}\cdot\mathbf{R}_{inv}\cdot\mathbf{R} = \mathbf{R} \ (\varepsilon \le \varepsilon_m) \text{ and } \mathbf{R}_{inv}\cdot\mathbf{R}\cdot\mathbf{R}_{inv} = \mathbf{R}_{inv} \text{ (for all } \varepsilon). \tag{23}$$

C. Minimization of Orbit Error

Orbit correction when the number of BPMs M is not larger than the number of coupled channels C ($\le$ min(M, N)) is trivial since the solution that satisfies Eq. (17) always exists. Let us now consider the case when M is larger than C, the maximum number that does not saturate the corrector strengths, and let $\Delta\mathbf{x}$ be the initial orbit error. Then after applying the correction $\Delta\boldsymbol{\theta}$ given by Eq. (18), the new difference orbit $\Delta\mathbf{x}'$, using Eqs. (11) and (12), is

$$\Delta\mathbf{x}' = (\mathbf{1} - \mathbf{R}\cdot\mathbf{R}_{inv})\cdot\Delta\mathbf{x} = \mathbf{U}\cdot(\mathbf{1} - \mathbf{W}\cdot\mathbf{W}_{inv})\cdot\mathbf{U}^T\cdot\Delta\mathbf{x}, \tag{24}$$

or, in the t-BPM space,

$$\Delta\mathbf{x}'^t = \mathbf{U}^T\cdot\Delta\mathbf{x}' = (\mathbf{1} - \mathbf{W}\cdot\mathbf{W}_{inv})\cdot\Delta\mathbf{x}^t. \tag{25}$$

Since the transformation conserves vector norm, Eq. (25) gives

$$\left|\Delta\mathbf{x}'\right| = \left|\Delta\mathbf{x}'^t\right| = \left(\sum_{i=C+1}^{M} |\Delta x'^t_i|^2\right)^{1/2}. \tag{26}$$

In Eq. (26), the position error $\Delta x'^t_i$ is reduced to zero for the coupled t-BPMs ($1 \le i \le C$) after correction, while it is conserved for the decoupled t-BPMs ($C + 1 \le i \le M$). Therefore, the orbit error cannot be reduced further than given by Eq. (26) unless C is increased, e.g., by optimizing the corrector strengths. This is also proven by showing that the corrector strengths are not changed any more. From Eq. (23),

$$\Delta\boldsymbol{\theta}' = \mathbf{R}_{inv}\cdot\Delta\mathbf{x}' = (\mathbf{R}_{inv} - \mathbf{R}_{inv}\cdot\mathbf{R}\cdot\mathbf{R}_{inv})\cdot\Delta\mathbf{x} = \mathbf{0}. \tag{27}$$

Particularly, with C equal to N, Eq. (26) is the absolute minimum beyond which no further orbit correction is possible by any method. However, in reality, error in the measurement of the response matrix $\mathbf{R}$, changes in the machine condition, and external perturbations cause residue in the closed orbit error. Correction of this error is done by AC orbit correction with appropriate bandwidth.

D. Optimization of Corrector Strength

When the number of correctors N is larger than C, the number of coupled channels, the correctors can then be optimized in various ways. Between successive corrections of the closed orbit, some of the correctors can be close to saturation, thus preventing any further corrections. In this case, if N is larger than C, the decoupled t-correctors can be used to relieve those correctors.

Let $\mathbf{V}_s$ be the submatrix of $\mathbf{V}$ that corresponds to the decoupled t-correctors. That is,

$$V_{sij} = V_{i,j+C}. \quad (1 \le i \le N, 1 \le j \le N\text{–}C) \tag{28}$$

The desired corrector strength change, $\Delta\boldsymbol{\theta}_s$, is transformed in the subspace of t-correctors spanned by the corrector basis vectors v_j (C+1 ≤ j ≤ N) and then inverse-transformed. The resulting $\Delta\boldsymbol{\theta}_s'$ given by

$$\Delta\boldsymbol{\theta}_s' = \mathbf{V}_s \cdot \mathbf{V}_s^T \cdot \Delta\boldsymbol{\theta}_s \tag{29}$$

will then be the closest to the $\Delta\boldsymbol{\theta}_s$ while disturbing the orbit the least. As a special case, when $\Delta\boldsymbol{\theta}_s = \mathbf{0}$, we have

$$|\Delta\boldsymbol{\theta}| = |\Delta\boldsymbol{\theta}^t| = \left(\sum_{j=1}^{C} |\Delta\theta_j^t|^2\right)^{1/2} \tag{30}$$

since $\Delta\theta_j^t = 0$ for the decoupled t-correctors (C + 1 ≤ j ≤ N). That is, $|\Delta\boldsymbol{\theta}|$ given by Eq. (30) is the minimum value possible. Particularly, when C = N, it is the absolute minimum among all solutions that satisfy Eq. (17).

In a similar manner, if $\boldsymbol{\theta}$ is the current corrector strength, $\boldsymbol{\theta}'$ given by

$$\boldsymbol{\theta}' = \mathbf{R}_{inv} \cdot \mathbf{R} \cdot \boldsymbol{\theta} \tag{31}$$

will minimize the overall corrector strength. In case N > C, further optimization can be done by applying Eq. (29).

GLOBAL ORBIT FEEDBACK

Orbit correction experiments based on the SVD algorithm were conducted on the X-ray ring of the National Synchrotron Light Source (NSLS) for DC and on SPEAR at Stanford Synchrotron Radiation Laboratory (SSRL) for DC and AC. For DC correction, integral control with full correction was used, while for AC correction, proportional and integral (PI) control was used. Analysis of the global orbit feedback on the APS storage ring will also be discussed in this section.

A. Global DC Orbit Correction on the NSLS X-ray Ring[18]

We used all of the 48 (M) BPMs and 39 (N) correctors available for orbit correction. The nominal vertical tune of the machine is $\nu_v = 6.2$. The response matrix was measured as the ratio of the beam motion in mm and the applied current on the corrector magnets in amperes.

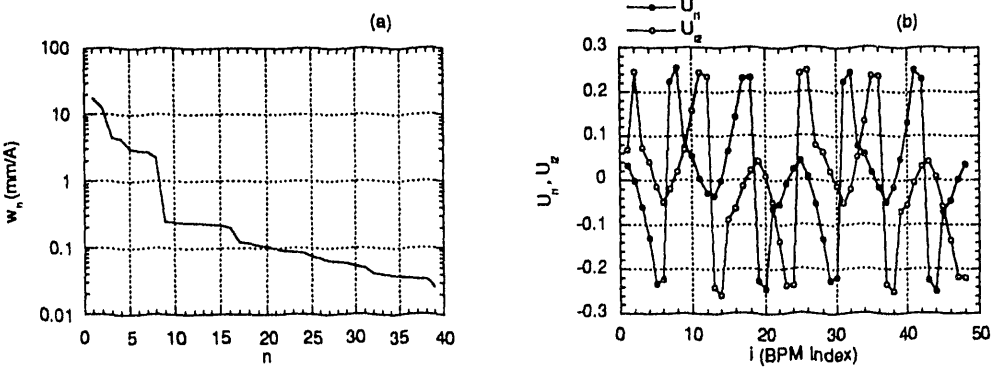

Fig. 7: (a) Plot of the eigenvalues of the response matrix for the NSLS X-ray ring in the vertical plane. $\varepsilon_m = 1.47\times10^{-3}$. (b)The basis vectors U_{i1} and U_{i2} of the NSLS X-ray ring for the most strongly coupled channels.

Figure 7(a) shows the eigenvalues w_n ($1 \le n \le 39$) for the NSLS X-ray ring, with $\varepsilon_m = 1.47\times10^{-3}$. The BPM basis vectors U_{i1} and U_{i2} ($1 \le i \le 48$) for the most strongly coupled channels are shown in Fig. 7(b). These two vectors exhibit pseudo-periodicity of the integer tune 6 and are shifted in phase by approximately 90 degrees. This indicates that the two channels will primarily correct m = 6 harmonic mode.

The result of orbit correction using 35 eigenvalues on the NSLS X-ray ring is shown in Fig. 8. The initial r.m.s. orbit error was 138 μm, which was reduced to 61 μm after correction. A few iterations were necessary before the r.m.s. error settled down to this value, possibly due to changes in machine condition and error in the response matrix measurement. The corrector current changes ranged from -4.56 A to 2.45 A, with an r.m.s. value of 1.47 A. Some of the corrector power supplies got close to, but did not reach, saturation at the maximum current of 10 A. Including more eigenvalues would trip off some of the power supplies and was not tried.

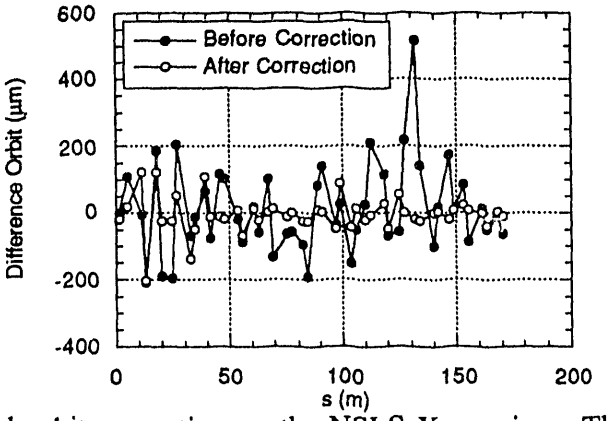

Fig. 8: DC global orbit correction on the NSLS X-ray ring. The r.m.s. orbit error relative to the reference orbit is 137 μm and 61 μm before and after correction, respectively. Thirty-five eigenvalues out of 39 were used.

B. Global DC Orbit Correction on SPEAR, SSRL[18]

For SPEAR at SSRL, all of the 26 BPMs and 30 correctors available for orbit correction were used. The nominal vertical tune of the machine is $\nu_y = 6.72$. As shown in Fig. 9(a), the response matrix is nearly singular, and the weakest four channels (n = 23 – 26) may not be usable unless the power supplies are very robust. ε_m of the response matrix is 4.43×10^{-4}.

We tried to bring the orbit as close as possible to the electrical centers of the BPMs, which were used as the reference for orbit correction. After each correction, the RESOLVE[19] program was used to fit the measured orbit to the machine model. This enabled us to locate some of the BPMs with significant offsets and remove them from orbit correction. Using this procedure, 9 out of 26 were removed, and the result is shown in Fig. 9(b). The r.m.s. orbit error was reduced from 780 μm to 215 μm at the locations of the 17 remaining BPMs using 15 eigenvalues. Two channels had to be decoupled to avoid power supply saturation resulting from the misalignment of a BPM with the center of an adjacent quadrupole. This led to the kink in the orbit between the 9th and 10th BPMs.

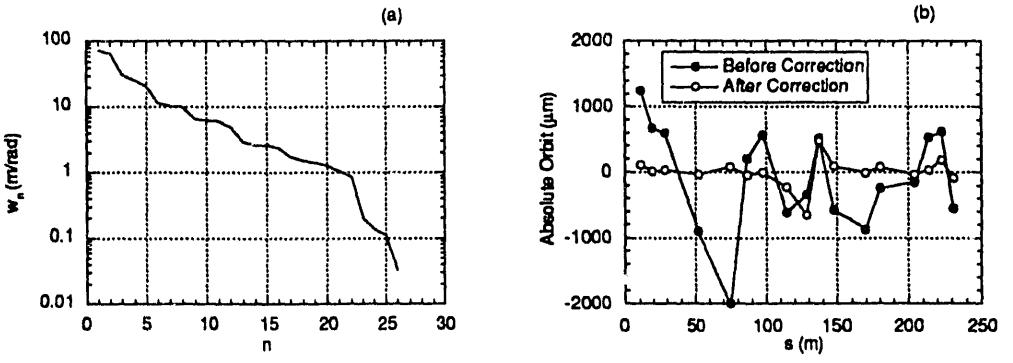

Fig. 9: (a) Plot of the eigenvalues of the response matrix for SPEAR in the vertical plane. $\varepsilon_m = 4.43\times10^{-4}$. (b) DC global absolute orbit correction at SPEAR, SSRL. The r.m.s. orbit error relative to the vacuum chamber center is 780 μm and 215 μm before and after correction, respectively. Fifteen eigenvalues out of 17 were used.

C. Global AC Orbit Correction on SPEAR, SSRL

Figure 10 shows the schematic of the setup for global AC beam position feedback experiments conducted on SPEAR at SSRL. Ten BPMs were used to detect beam motion and 16 correctors were used for closed orbit correction. For beam position measurement, the signals from BPM striplines were multiplexed and processed by an analog circuit and then digitized by an ADC with 12-bit resolution and ±5V full scale. The beam position was then measured in dimensionless units as:

$$x = 65{,}536 \times \frac{V_1 - V_2 - V_3 + V_4}{V_1 + V_2 + V_3 + V_4} \quad \text{and} \quad y = 65{,}536 \times \frac{V_1 + V_2 - V_3 - V_4}{V_1 + V_2 + V_3 + V_4}. \qquad (32)$$

The constant 65,536 was multiplied in order to convert the signal ratio to an integer.

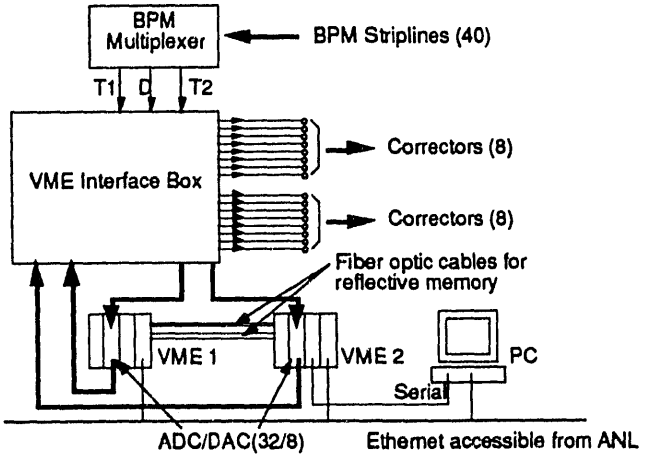

Fig. 10: Schematic of the setup for global AC beam position feedback experiments on SPEAR, SSRL.

The corrector power supply was controlled through a DAC with 12-bit resolution and ±5V full scale corresponding to ±60A current range. The response matrix was measured in dimensionless units as the ratio of the beam motion and corrector strength changes. The response matrix is not singular and the eigenvalues ranged from 9.152 to 0.242 giving $\varepsilon_m = 0.0264$.

The result of closed orbit feedback is shown in Fig. 11 (a) in time domain and (b) in frequency domain. The sampling frequency was 37 Hz and the open loop bandwidth was set at 1% of the sampling frequency, that is, 0.37 Hz. Since the proportional gain K_P is 3, closed loop bandwidth of approximately 1 Hz can be expected, which is in good agreement with the result shown in Fig. 7(b). This implies that the orbit correction bandwidth for the APS with 4-kHz sampling frequency will be approximately 100 Hz.

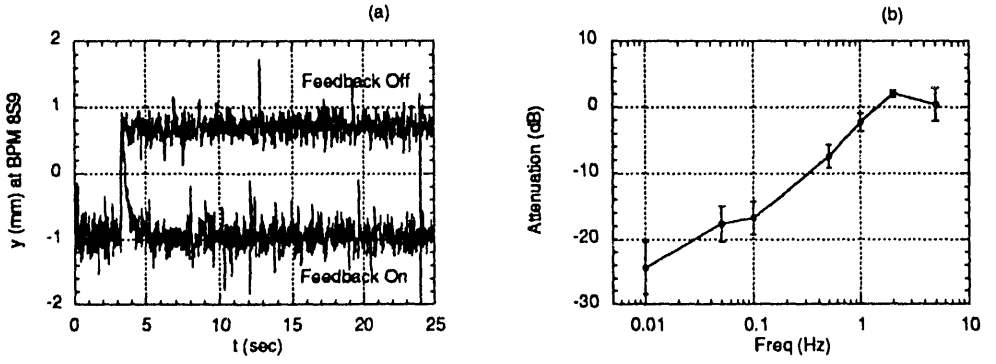

Fig. 11: Result of global orbit feedback on SPEAR, SSRL in (a) time domain and (b) frequency domain. The parameters used were: $K_p = 3$, $K_I = 0.05$, $K_D = 0$, $F_s = 37$ Hz, and $f_b = 0.37$ Hz.

D. Analysis of the APS Storage Ring

In this section, we will analyze global orbit correction for the APS storage ring in the vertical plane. There are 40 sectors in the machine and each sector has nine BPMs (total 360) and eight correctors (total 320) available for global orbit correction. The distribution of BPMs and correctors is identical for all sectors.

Figure 12(a) shows the eigenvalues w_n ($1 \le n \le 320$) in descending order when all BPMs and correctors are used. The maximum and minimum values are 1.140×10^{3} and 9.126×10^{-2} ($\varepsilon_m = 8.005\times10^{-5}$) in units of m/rad, respectively. The machine periodicity is exhibited in the discontinuous changes of w_n at every 40. The large decrease at $n = 240$ indicates that 80 of the correctors are almost redundant and therefore do not contribute much to orbit correction except to reduce overall corrector strengths. These correctors have the smallest values of the function

$$E(j) = \sum_n w_n V_{jn}^2. \quad (1 \le j \le 320) \tag{33}$$

When those correctors are removed, ε_m becomes 6.656×10^{-4}.

The function E(j) is a measure of the efficiency of the j-th corrector. A similar function can be defined for the BPMs and these functions can be used to select a subset of BPMs and correctors with the condition that ε_m be maximized.

Figure 12(b) shows the plot of the BPM basis vectors U_{i1} and U_{i2} as functions of the BPM index i. These vectors are mutually orthogonal and correspond to the largest eigenvalues w_1 and w_2 equal to 1.140×10^3 m/rad. They also have the same frequency as the integer tune ($\nu_V = 14.2987$) of the machine, which means that perturbation with the harmonic number 14 can be corrected the most efficiently. The first two corrector basis vectors V_{j1} and V_{j2} show similar behavior.

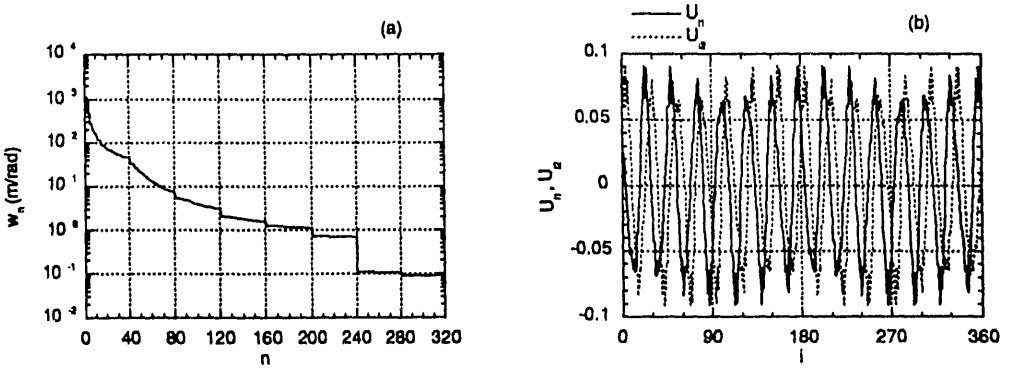

Fig. 12: (a) Plot of the eigenvalues in descending order for the APS storage ring with M = 360 and N = 320 in the vertical plane. $\varepsilon_m = 8.005 \times 10^{-5}$. (b) The BPM basis vectors U_{i1} and U_{i2} ($1 \le i \le 360$) for the most strongly coupled channels ($w_1 = w_2 = 1.140 \times 10^3$ m/rad) in the vertical plane ($\nu_V = 14.2987$) for the APS storage ring.

For global AC feedback, the same number (M = N = 40) of BPMs and correctors are used for both the horizontal and vertical planes. The ring has 40 sectors and the BPMs and correctors are located an equal distance apart. As a result, correspondence exists between the SVD eigenmodes and harmonic modes, as is shown in Fig. 13. The ten largest SVD eigenvalues were used for orbit correction in the horizontal plane and noise attenuation for (a) SVD eigenmodes and (b) harmonic modes was calculated. With the betatron tune $\nu_H = 35.2154$, the harmonic modes m = 5 and 35 correspond to the largest eigenvalues $w_{1,2} = 181$ m/rad. Similar correspondence can be found for other modes.

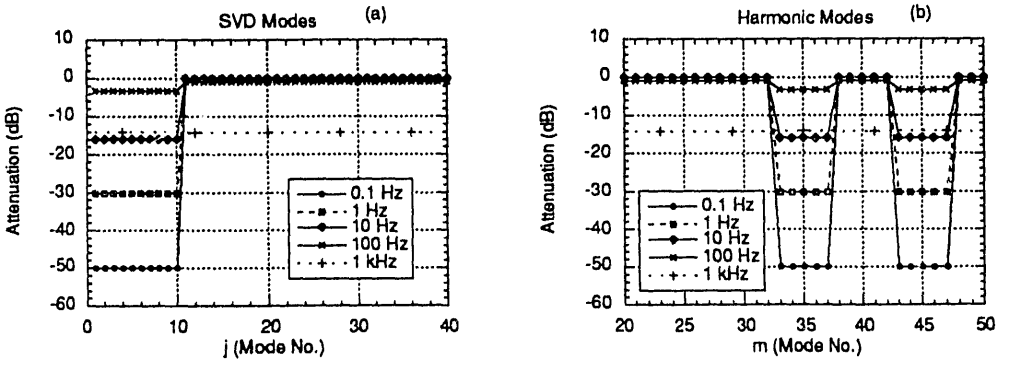

Fig. 13: Correspondence between the (a) SVD eigenmodes and (b) harmonic modes for global AC feedback in the horizontal plane of the APS storage ring. The ten largest SVD eigenvalues are used for orbit correction in the horizontal plane.

LOCAL ORBIT FEEDBACK

The local feedback systems primarily handle isolated noise on the X-ray beamline and will employ four-magnet bumps to control both the position and the angle of the X-ray source point as shown in Fig. 14. For the bending magnet radiation, the source point is placed at the center of the main dipole, while for the insertion device, the radiation is along the extension of the line adjoining the beam position at the location of bump magnets 2 and 3.

A. Closed Loop Feedback on a Single Local Beamline

The position and angle of the radiation source are monitored using a set of two X-ray photon beam position monitors at the end of the beamline, which registers the photon beam positions (y_{b1} and y_{b2}) at longitudinal locations x_{b1} and x_{b2}. For insertion device beamlines, two additional rf miniature BPMs may be used as complement to the X-ray BPMs. The relation between the three-magnet bump strengths δ_a and δ_b and the photon beam positions y_{b1} and y_{b2} is given by[20]

$$\begin{pmatrix} y_{b1} \\ y_{b2} \end{pmatrix} = \mathbf{D}\cdot\mathbf{A}\cdot\begin{pmatrix} \delta_a \\ \delta_b \end{pmatrix}, \tag{34}$$

where

$$\mathbf{A} = \sqrt{\beta_2\beta_3}\sin(\phi_3 - \phi_2)\begin{pmatrix} K_{3a} & 0 \\ 0 & K_{2b} \end{pmatrix} \tag{35}$$

and

$$\mathbf{D} = \frac{1}{x_{s3} - x_{s2}}\begin{pmatrix} -|x_{b1} - x_{s3}| & |x_{b1} - x_{s2}| \\ -|x_{b2} - x_{s3}| & |x_{b2} - x_{s2}| \end{pmatrix}. \tag{36}$$

K_{3a} is the relative weight of magnet 3 in the bump a, and K_{2b} is the relative weight of magnet 2 in the bump b. β_2 and β_3 are the β-function values at bump magnet locations 2 and 3, and ϕ_2 and ϕ_3 are the corresponding betatron phases. In order to have local bump closure, the relative weights K_{ij} (i = 1,2,3, and j = a, b) must satisfy

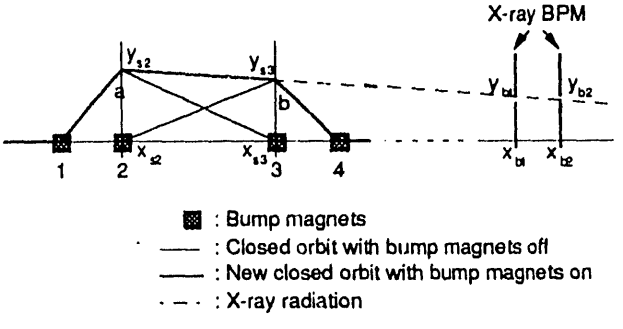

Fig. 14: Four-magnet bump to control the position and the angle of the X-ray radiation, which comprises two three-magnet bumps a (magnets 1, 2, and 3) and b (magnets 2, 3, and 4). x and y are coordinates for the longitudinal distance and the beam position, respectively.

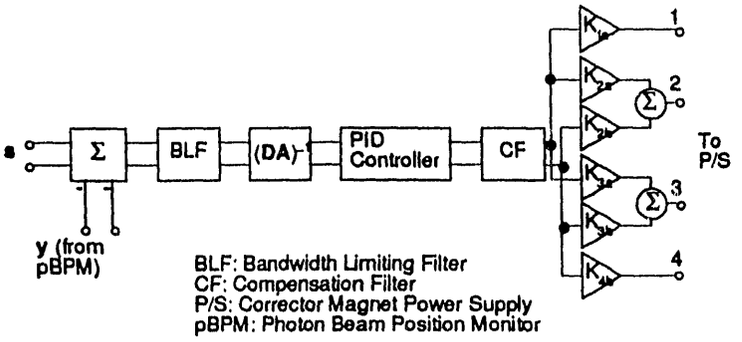

Fig. 15: Schematic of the local beam position feedback using DSP.

$$\frac{K_{2a}}{K_{1a}} = -\left(\frac{\beta_1}{\beta_2}\right)^{1/2} \frac{\sin(\phi_3 - \phi_1)}{\sin(\phi_3 - \phi_2)}, \quad \frac{K_{3a}}{K_{1a}} = \left(\frac{\beta_1}{\beta_3}\right)^{1/2} \frac{\sin(\phi_2 - \phi_1)}{\sin(\phi_3 - \phi_2)} \tag{37}$$

and

$$\frac{K_{3b}}{K_{2b}} = -\left(\frac{\beta_2}{\beta_3}\right)^{1/2} \frac{\sin(\phi_4 - \phi_2)}{\sin(\phi_4 - \phi_3)}, \quad \frac{K_{4b}}{K_{2b}} = \left(\frac{\beta_2}{\beta_4}\right)^{1/2} \frac{\sin(\phi_3 - \phi_2)}{\sin(\phi_4 - \phi_3)}. \tag{38}$$

Equation (34) relates the strength of the bump magnets and the photon beam motion and is the basis of the closed loop feedback. The schematic is shown in Fig. 15. The vector **s** is the control signal for the photon beam position vector **y** (y_{b1} and y_{b2}), whose difference is fed to the digital signal processor. The output from the matrix $(\mathbf{D}\cdot\mathbf{A})^{-1}$ is the three-magnet bump strength δ_a and δ_b, which is split to the four power supplies for the bump magnets.

B. Unified Global and Local Feedback Systems

Even though the local bump as shown in Fig. 14 is designed to be truly local and not perturb other local systems or the global system, bump coefficient error, magnet field error, and eddy current effect can cause local bump closure error and

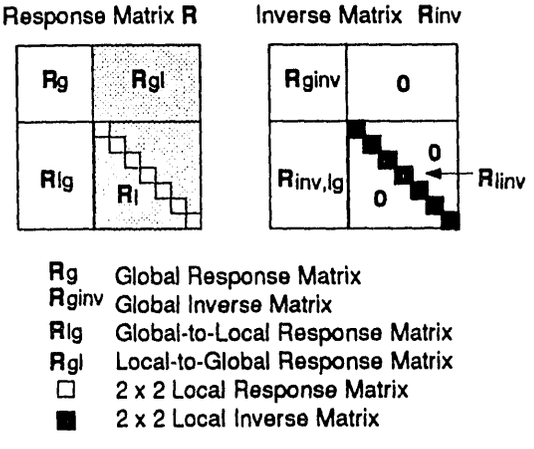

Fig. 16: Response matrix and its inverse for the unified feedback system.

thus global orbit perturbation. For multiple such local feedback systems, the resulting cross-talk among them can lead to oscillation and instability. Even though this effect can be partially canceled by the global feedback system, it will unnecessarily perturb the local orbits as well. As a result, the orbit correction efficiency will decrease.

One can find a way to resolve this by considering the global and local feedback systems as a single, unified feedback system. Consider the full response matrix **R** and its inverse as shown in Fig. 16. For the case of no local bump closure error, we will have the local-to-global matrix $\mathbf{R}_{gl} = \mathbf{0}$. In general, the global-to-local matrix $\mathbf{R}_{lg}$ is not zero. For independent operation of the global and local feedback systems, the off-diagonal matrix $\mathbf{R}_{inv,lg}$ is equal to zero, and it can be easily seen that $\mathbf{R}\cdot\mathbf{R}_{inv}$ has off-diagonal elements which represent the global-to-local interaction. This uni-directional interaction is canceled out by putting

$$\mathbf{R}_{inv,lg} = -\mathbf{R}_{linv}\cdot\mathbf{R}_{lg}\cdot\mathbf{R}_{ginv}. \tag{39}$$

The physical interpretation of Eq. (39) can be given as follows. $\mathbf{R}_{ginv}$ is the response of the global correctors to global orbit perturbation, $\mathbf{R}_{lg}$ is the local orbit perturbation due to global correctors, and $\mathbf{R}_{linv}$ is the response of the local correctors to local orbit perturbation. The matrix product $\mathbf{R}_{linv}\cdot\mathbf{R}_{lg}\cdot\mathbf{R}_{ginv}$ is then the response of the local correctors to global orbit perturbation and $\mathbf{R}_{inv,lg}$ in Eq. (39) compensates for the action of the global feedback system on the local orbits, resulting in maximum orbit correction efficiency. Figure 17 shows improvement of local orbit correction efficiency when the global and local feedback systems are unified. The noise sources are SVD eigenmodes. Random field error less than 2% and orbit deviation less than 3 mm were assumed with the vacuum chamber eddy current taken into account.

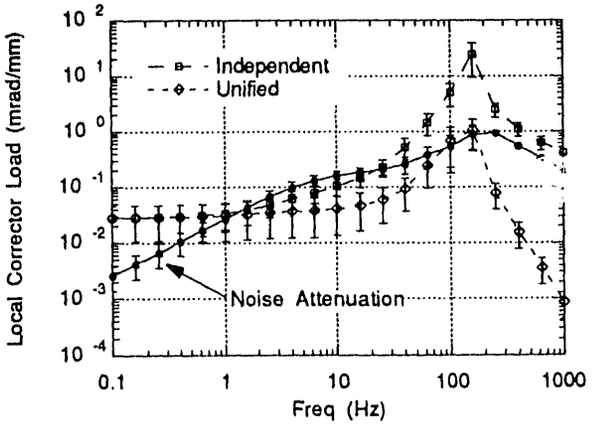

Fig. 17: Improvement of local orbit correction efficiency for the unified system. The noise sources are SVD eigenmodes. Random field error less than 2% and orbit deviation less than 3 mm were assumed with the vacuum chamber eddy current taken into account.

SYSTEM CONFIGURATION

In this section, we will discuss the hardware and software configuration for the APS beam position feedback system.

A. Hardware

For digital feedback systems, sampling frequency or the number of corrections per unit time, is of fundamental importance. The correction bandwidth of a closed loop feedback system is largely limited by the sampling frequency. For the APS storage ring, the design sampling frequency is 4 kHz for both the global and local feedback systems, and therefore, one feedback loop should complete within 250 μs with no overlap in time among various processes. The time budget for beam position feedback system is:

Data acquisition from BPMs ≈ 50 μsec
Calculation of corrector strengths by DSP ≈ 100 μsec
Corrector power supply control ≈ 100 μsec

In order to achieve this high sampling frequency, we will use digital signal processors and fiber-optically networked high-speed reflective memory boards (26 Mbits/sec transfer rate). These are distributed around the ring in 20 VME crates interfaced to BPM processors and power supply controllers through optical fibers as shown in Fig. 18. The DSP boards and reflective memory boards are commercially available. The interface boards for the BPMs and correctors are being designed and tested in-house.

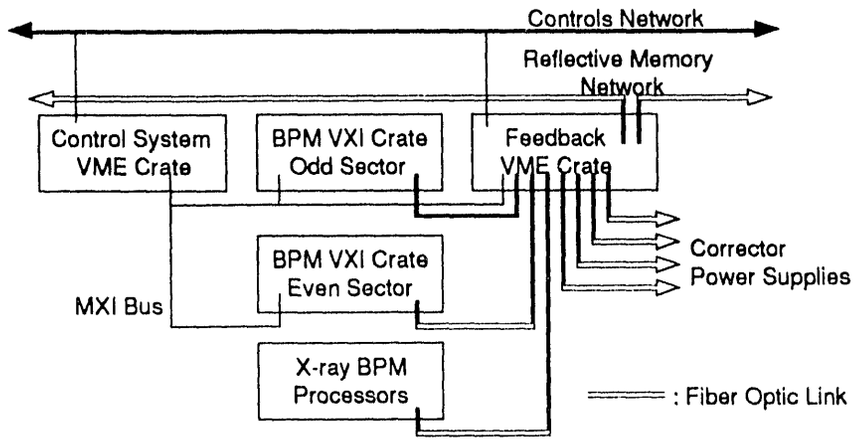

Fig. 18: Hardware configuration of the beam position feedback system. There are 20 feedback system crates distributed around the APS storage ring.

B. Software

The software configuration is shown in Fig. 19. The beam position feedback system is interfaced through the APS control system via EPICS (Experimental Physics and Industrial Control System) or directly to the Motorola 68040 VME crate CPUs and Texas Instruments' TMS320C30 DSPs. All the real-time codes including data I/O interface with the BPMs and correctors will run on the DSPs, while the crate CPUs will serve as interface to the control system and users.

Given the complexity of the system and in order to take advantage of built-in flexibility, we are currently developing software for automatic code generation. It will take an input file containing information on the system configuration, generate all the necessary codes for crate CPUs and DSPs, and download them to the processors.

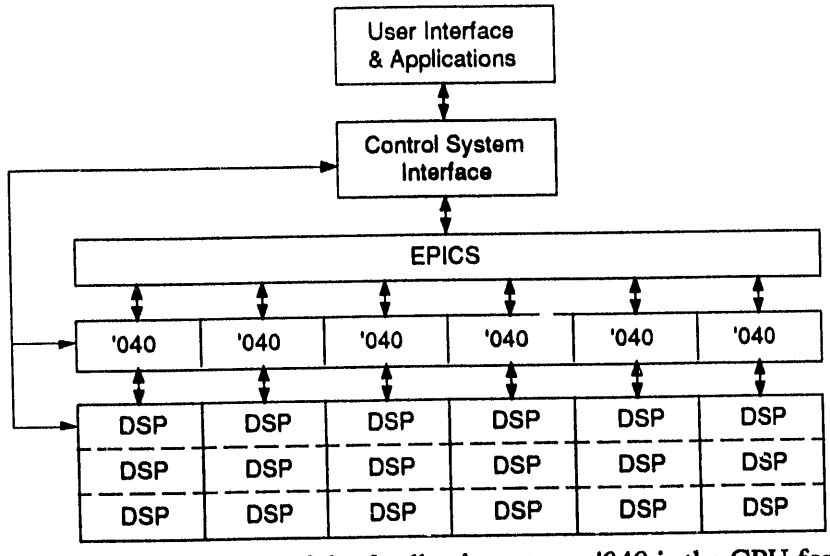

Fig. 19: Software configuration of the feedback system. '040 is the CPU for the VME crate running the real-time operating system VxWorks. The DSP is Texas Instruments' TMS320C30 and will run real-time codes including data I/O interface.

SUMMARY AND STATUS

The design principle of the APS beam position feedback system consists of an orbit correction algorithm based on singular value decomposition (SVD) of the response matrix and digital signal processing (DSP) with a proportional, integral, and derivative (PID) control algorithm. SVD transforms the response matrix such that the matrix product of the machine response and its inverse for orbit correction becomes a diagonal matrix. This renders the feedback system into multiple non-interacting closed loop feedback systems, to which we can apply the theory of single-channel digital feedback. These basic design concepts were verified through experiments on the NSLS X-ray ring and SPEAR at SSRL.

As a departure from the conventional approach to beam position feedback, the global and local feedback systems are combined into a single, unified feedback system. The effect of local bump closure error in the local systems is reduced through orbit correction by the global feedback system. This approach removes the undesirable interaction between the global and local feedback systems and maximizes orbit correction efficiency.

At the time of this writing, we are expecting delivery of commercial DSP boards and reflective memory boards. The corrector power supply interface board has been designed and is ready for field testing. The interface boards for the rf BPMs and X-ray BPMs are in the design stage and prototypes will be built in the near future.

ACKNOWLEDGMENTS

The author would like to thank G. Decker, L. Emery, K. Evans, Jr., J. Kirchman, F. Lenkszus, and A. J. Votaw of the APS project for their contributions to this work. Thanks also go to J. Galayda, M. Knott, A. Lumpkin, and L. Teng for their support and interest. J. Safranek, I. So, and Y. Tang at NSLS and R. Hettel, W. J.

Corbett, M. Lee, J. Sebek, and J. Yang at SSRL are to be thanked for their collaboration on the measurements.

REFERENCES

1. R. O. Hettel, "Beam Steering at the Stanford Synchrotron Radiation Laboratory," IEEE Trans. Nucl. Sci., **NS-30**, No. 4, p. 2228, 1983.
2. R. J. Nawrocky et al., "Automatic Beam Steering in the NSLS Storage Rings Using Closed Orbit Feedback," Nucl. Instr. and Meth., **A266**, p. 164, 1988.
3. L. H. Yu et al., "Real Time Closed Orbit Correction System," *Proceedings of IEEE Particle Accelerator Conference*, Chicago, 1989.
4. D. Bulfone et al., "Design Considerations for the Elettra Beam Position Feedback Systems," *Proceedings of the 2nd European Particle Accelerator Conference*, Nice, 1990.
5. Y. Chung, L. Emery, and J. Kirchman, "Compensation for the Effect of Vacuum Chamber Eddy Current by Digital Signal Processing for Closed Orbit Feedback," *Proceedings of IEEE Particle Accelerator Conference*, Washington, D.C., 1993.
6. A. Peled and B. Liu, *Digital Signal Processing*, John Wiley & Sons, 1976.
7. Y. Chung, L. Emery, and K. Kirchman, "Digital Signal Processing for Beam Position Feedback," LS Note 202, ANL, 1992.
8. Y. Chung and J. Galayda, "Effect of Eddy Current in the Laminations on the Magnet Field," LS Note 200, ANL, 1992.
9. G. H. Golub and C. Reinsch, "Singular Value Decomposition and Least Squares Solutions," Numer. Math. **14**, pp. 403–420, 1970, and references therein.
10. G. E. Forsythe, M. A. Malcolm, and C. B. Moler, *Computer Methods for Mathematical Computations*, Prentice-Hall, Englewood Cliffs, N.J., 1977.
11. J. J. Dongarra, et al., *LINPACK User's Guide*, Chapter 11, Society for Industrial and Applied Mathematics, Philadelphia, 1979.
12. *MATLAB™ User's Guide*, The Mathworks, Inc., p. 3-178, 1990.
13. K. J. Kleman, "Beam Diagnostics and Control at Aladdin," Nuclear Inst. and Meth., **A266**, p. 172, 1988.
14. Y. Chung, G. Decker, and K. Evans, Jr., "Closed Orbit Correction Using Singular Value Decomposition of the Response Matrix," *Proceedings of IEEE Particle Accelerator Conference*, Washington, D.C., 1993.
15. M. Sands, "The Physics of Electron Storage Rings - An Introduction," SLAC-121, 1970.
16. W. Press et al., *Numerical Recipes in C*, Cambridge University Press, p. 60, 1989.
17. *Mathematica™*, Wolfram Research, Inc., p. 454, 1988.
18. Y. Chung, et al., "Global DC Closed Orbit Correction Experiments on the NSLS X-ray Ring and SPEAR," *Proceedings of IEEE Particle Accelerator Conference*, Washington, D.C., 1993.
19. W. J. Corbett, M. J. Lee, and Y. Zambre, "Automatic Beamline Calibration Procedures," *Proceedings of the 3rd European Particle Accelerator Conference*, Berlin, p. 753, 1992.
20. S. Krinsky, et al., "Storage Ring Development at the National Synchrotron Light Source," BNL-46615, p. 58, 1991.

DATE

FILMED

12/22/93

END